Supporting information

Effects of Three-Dimensional Strain on Electric Conductivity in Au-Dispersed $Pr_{1.90}Ni_{0.71}Cu_{0.24}Ga_{0.05}O_{4+\delta}$

Junji Hyodo [1], Ken Tominaga [1], Jong-Eun Hong [1], Shintaro Ida [1,2],

and Tatsumi Ishihara [, 1,2]*

[1]Department of Applied Chemistry, Faculty of Engineering, Kyushu University,

Motooka 744, Nishi-ku, Fukuoka 819-0395, Japan

[2]International Institute for Carbon-Neutral Energy Research (WPI-I2CNER), Kyushu

University, Motooka 744, Nishi-ku, Fukuoka 819-0395, Japan

Detail analysis for XRD patterns

Since the splitting of (1 1 3) peak of 1 mol% Au/PNCG is expected from the curve in Figure 2(b), the peak deconvolution of XRD patterns in the 2θ region of 30-35 degrees is performed. Figure S1 shows the optimized results for curve fitting. Obviously,

the shoulder peaks at the both of 2 peaks in the 1 mol% Au/PNCG existed.
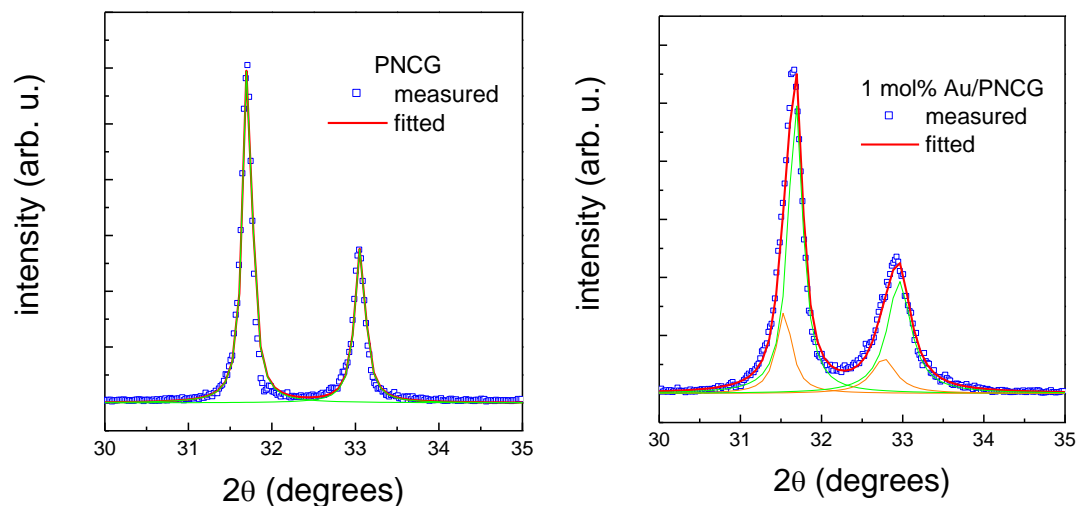
Figure S1 Curve fitting results of XRD pattern ($30^{o} < 2\theta < 35^{o}$) for PNCG (left) and 1 mol% Au/PNCG.

To consider the existence of the secondary phases, we thought the possible phases in the database (ICDD (PDF-2/ Release 2013 RDB)). The possible phases from the peak position of each shoulder peak are Pr_2CuO_4 (ICDD #01-070-5780) for the shoulder of (1 1 3) peak, $PrNiO_3$ (ICDD #01-079-2452) and $Pr_4Ni_3O_{9.85}$ (ICDD #00-050-0468) for the shoulder of (1 0 4)/(2 0 0) peaks, respectively. The peak positions of these phases without overlapping (the relative intensity (I/I_{max})>0.1) are shown in Figure S2. There seems to be no peaks of Pr_2CuO_4, $PrNiO_3$ and $Pr_4Ni_3O_{9.85}$. Therefore, it is concluded that observed shoulder peaks of (1 1 3) and (1 0 4)/(2 0 0) peaks are not explained by the secondary phase formation. As another possibility of this shoulder peak, the change in crystal structure with dispersing the Au particles was considered, because Pr_2NiO_4-based oxides have two phases reported, tetragonal and orthorhombic.[1] According to the standard references (tetragonal: ICDD;00-058-0850, orthorhombic: ICDD; 01-078-2196), it is also impossible to assign these shoulder peak with the crystal

structure change because there is no diffraction peak for orthorhombic structure at the 2theta of 21.55 degrees.
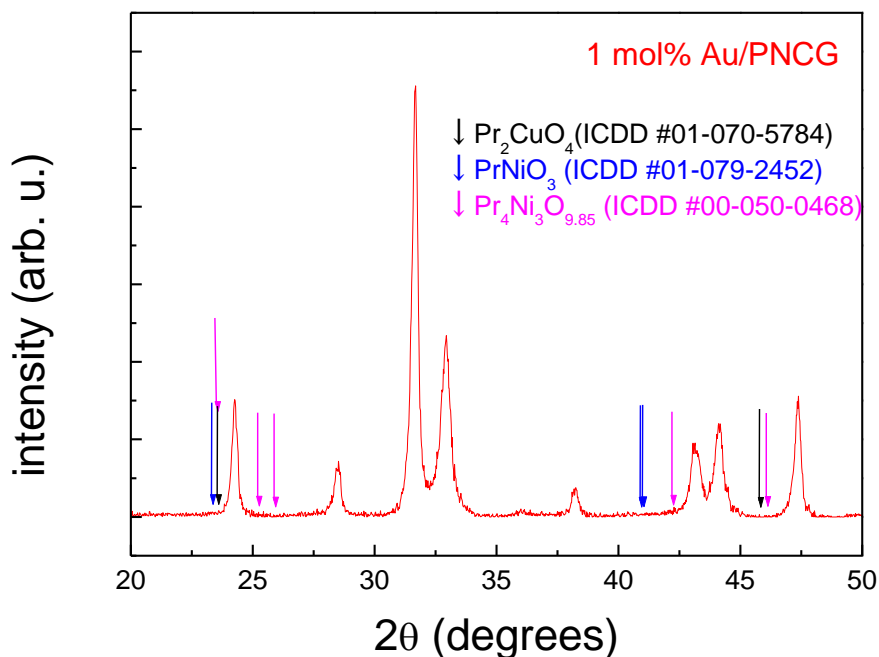
Figure S2 Wide-angle XRD pattern of 1 mol% Au/PNCG. The arrowheads indicate the peak position of possible phases which is suggested from the shoulder peak position of (1 1 3) and (1 0 4)/(2 0 0) peaks in Figure S1.

EDX analysis for composition

For the additional information of SEM-EDX analysis as shown in Figure 4 in the manuscript, the distribution of all consisting elements are shown in Figure S3. Obviously, distribution of Pr, Ni, Cu and Ga are quite uniform in the sample suggesting that no segregation of cation over the sample and so PNCG prepared is uniform in composition. Therefore, the shoulder peak observed on XRD patterns by dispersing Au is not assigned to PNCG with different composition, but from the broadening of the

peaks by distributed strain around Au particles.
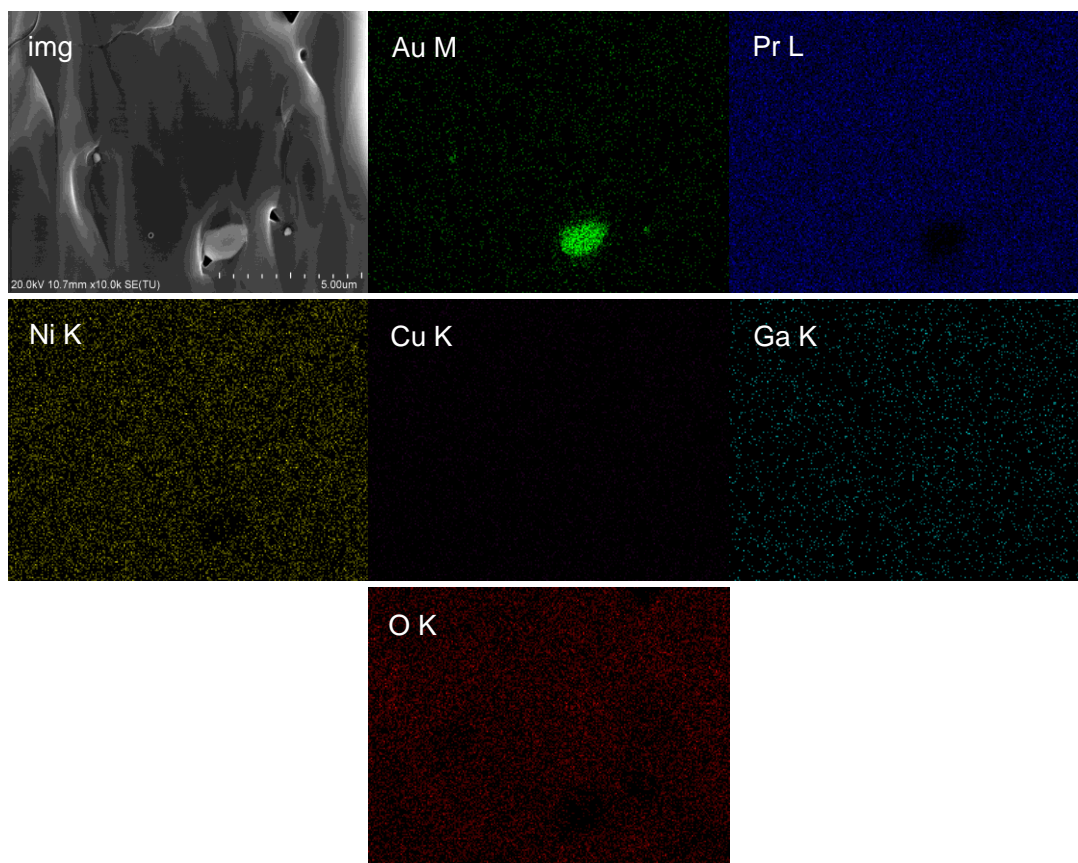
Figure S3 SEM-EDX images of 1 mol% Au/PNCG.

Rietveld Analysis of XRD patterns

In order to confirm the 3D strain, we prepared 0.5 mol% Au dispersed samples for the model samples. Furthermore, Rietveld analysis for x mol% Au/PNCG (x = 0, 0.5, 1) was performed to estimate the accurate lattice parameters. For the initial parameters of the refinement including space group, those which Yashima et al. used were also used in this study.[2] The fitting results were shown in Figure S4(a)−(c). The reliability factors for each analysis were reasonable but not small because XRD measurement was

performed using pellet (not powder), and also broadening the peak caused by distributed strain discussed in Figure S1. Figure S4(d) shows the lattice parameters as a function of dispersed Au amount. The refined lattice parameters increased with increasing Au amount. Therefore, it can be said that lattice parameter in all axes are increased with dispersion of Au. Furthermore, Vashook et al.[3] and Hücker et al.[4] have reported the relationship between the oxygen nonstoichiometry and the lattice parameter of the materials with K_2NiF_4 type structure. It is reported that the a- and b-axes and c-axis tends to be changed oppositely for keeping the lattice volume constant. Although the interstitial oxide ions were introduced into PNCG in our manuscript, all axes are increased by dispersion of Au. Therefore, as we expected, dispersion of Au metal particles could induce 3D strain into PNCG.
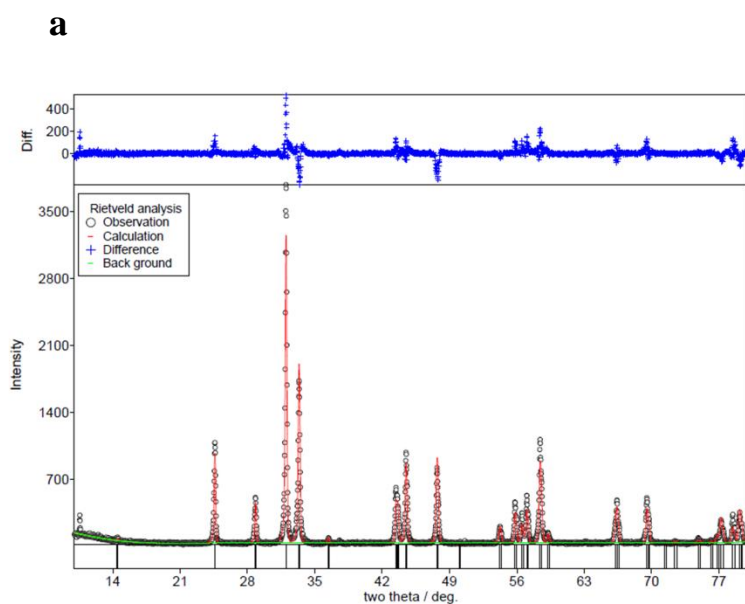
a

Note: Tetragonal space group $I4/mmm$, Number of formula units of $Pr_2Ni_{0.74}Cu_{0.21}Ga_{0.05}O_{4+\delta}$ in a unit cell: $Z = 2$. Unit cell parameters: $a = b = 3.7847(2)$ Å, $c = 12.3649(6)$ Å. Reliability factors in Rietveld analysis: $R_{wp} = 19.68$ %, $R_p = 15.42$ %, $R_e = 10.44$ %, $S = 1.8846$, $R_I = 12.86$ %, $R_F = 8.79$ %.

b
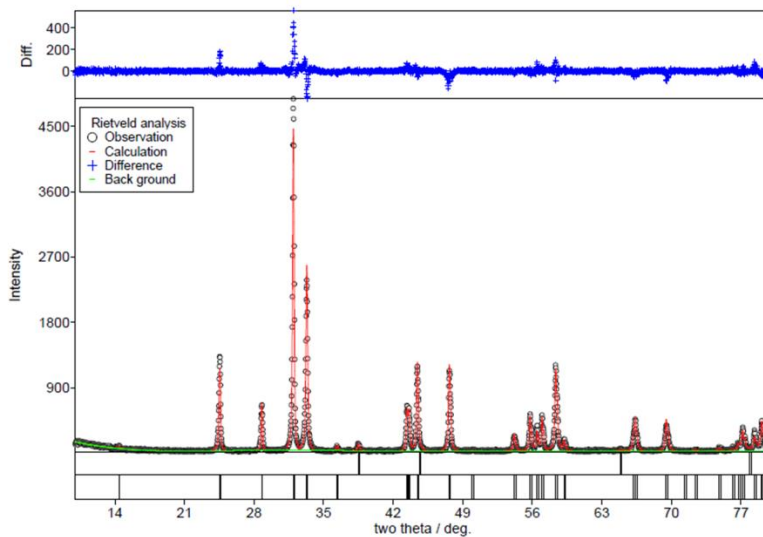
Note: Tetragonal space group $I4/mmm$, Number of formula units of $Pr_2Ni_{0.74}Cu_{0.21}Ga_{0.05}O_{4+\delta}$ in a unit cell: $Z = 2$. Unit cell parameters: $a = b = 3.81440(5)$ Å, $c = 12.4568(3)$ Å. Reliability factors in Rietveld analysis; $R_{wp} = 13.41$ %, $R_p = 10.16$ %, $R_e = 9.51$ %, $S = 1.4105$, $R_I = 5.71$ %, $R_F = 3.63$ %.

c
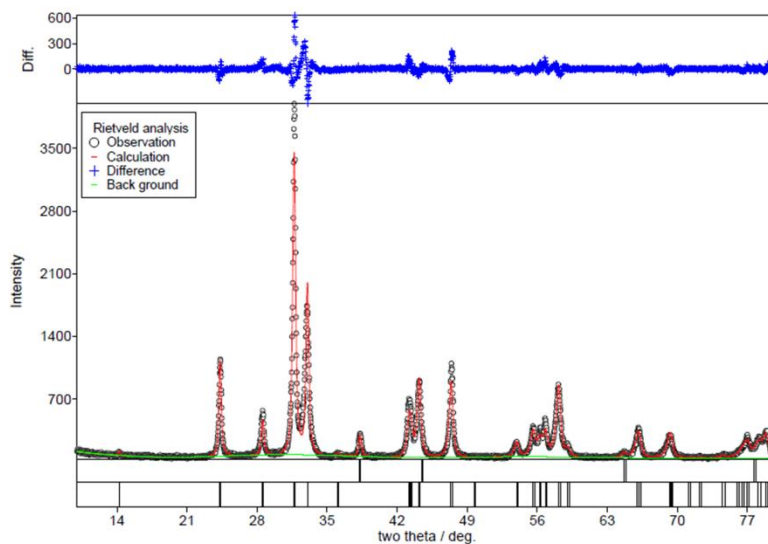
Note: Tetragonal space group $I4/mmm$, Number of formula units of $Pr_2Ni_{0.74}Cu_{0.21}Ga_{0.05}O_{4+\delta}$ in a unit cell: $Z = 2$. Unit cell parameters: $a = b = 3.8338(2)$ Å, $c = 12.5029(9)$ Å. Reliability factors in Rietveld analysis; $R_{wp} = 13.94$ %, $R_p = 11.14$ %, $R_e = 7.91$ %, $S = 1.7615$, $R_I = 4.63$ %, $R_F = 1.76$ %.

d
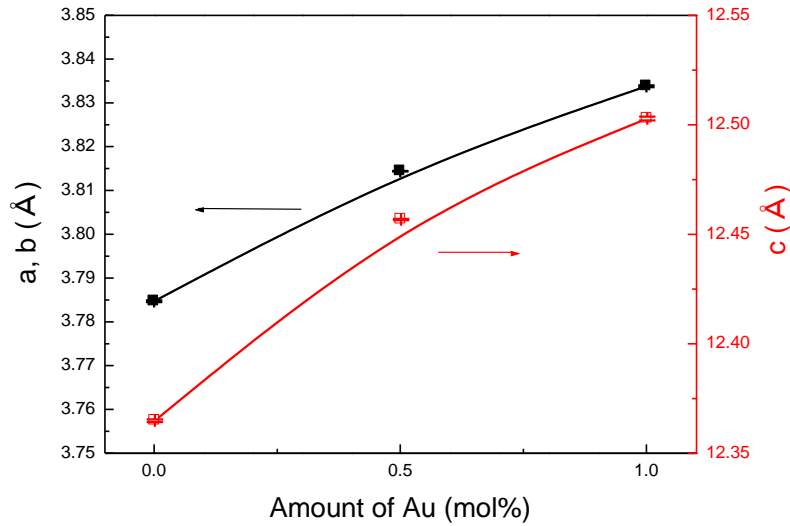
Figure S4 Rietveld refinement results for X-ray diffraction data of $Pr_2Ni_{0.74}Cu_{0.21}Ga_{0.05}O_{4+\delta}$ with (a) 0 mol%, (b) 0.5 mol% and (c) 1 mol% Au dispersion. (d) Estimated lattice parameters as a function of the amount of Au particles.

We tried to estimate the strain from the FWHM with Williamson-Hall method.[5] This method can separate the FWHM (denoted as $\Delta2\theta$) of diffraction peaks as the effect of crystal size and of strain, according to the equation below.

$$\Delta2\theta(cos\theta) = \frac{K \cdot \lambda}{L} + 2\varepsilon \cdot sin\theta$$

Figure S5 plots the $(\Delta2\theta)cos\theta$ as a function of $sin\theta$. The slope shows the strain, and obtained value was 0.190 ± 0.04 %. The changing ratio of lattice volume with dispersing the 1 mol% Au particle is 2.55 %. The difference between the estimated strain from the lattice volume and the FWHM was large. It seems likely that the larger peak shifts of XRD pattern than the diffraction peak broadening. In any case, both strain estimated from the lattice volume and the FWHM showed tensile strain by mechanical

7

or chemical effects.
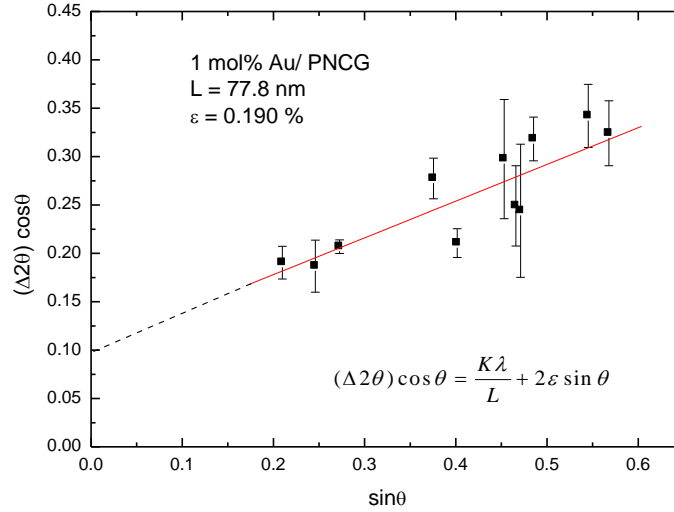
Figure S5 Williamson-Hall plots of 1 mol% Au/PNCG.

Effect of the sample density for the results of conductivity and Hall-effect

measurement

For the results of conductivity measurement, the obtained electrical conductivity

was corrected using the equation below in order to prove the enhancement with Au

dispersion is not related to the effect of the density.[6]

$$\frac{\sigma_{app}}{\sigma_{total}} = 2(0.01d_{rel} - 0.5)$$

σ_{app} is the observed conductivity, σ_{total} is the corrected conductivity, and d_{rel} is relative

density. Obtained relative density of the PNCG and 1 mol% Au/PNCG are 91 % and

95 %, respectively. Figure S6 shows the Arrhenius plots of electrical conductivity of

PNCG and 1 mol% Au/PNCG with and without the correction. Even though the

increment of electrical conductivity by the correction was obtained, the improvement

with Au dispersion is more significant than the density correction. This means the improved electrical conductivity cannot be explained with the density. Furthermore, we also correct the results of Hall-effect measurement which are shown in Figures 5 and 6 in the manuscript. Figure S7 shows the results of temperature dependence, and Figure S8 shows those of the oxygen partial pressure dependence, respectively. The tendencies of both results don't change significantly with density correction, indicating the effects of density for the electrical conductivity and Hall-effect measurement were ignorable.
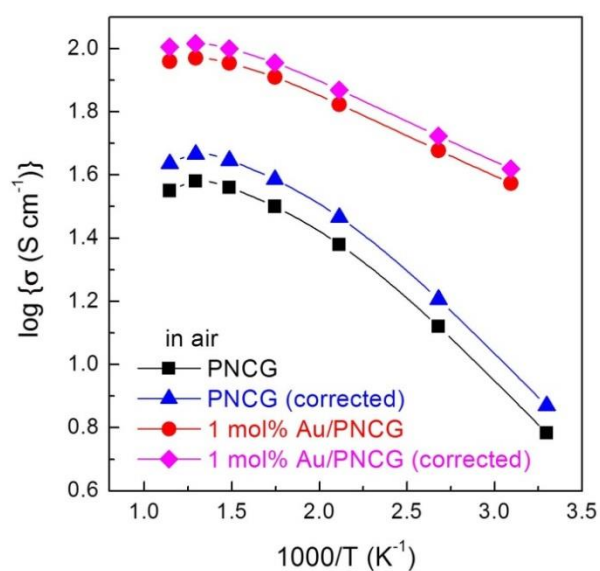
Figure S6 Arrhenius plots of conductivity with the density correction using Eq.(1).

a

b

c

d
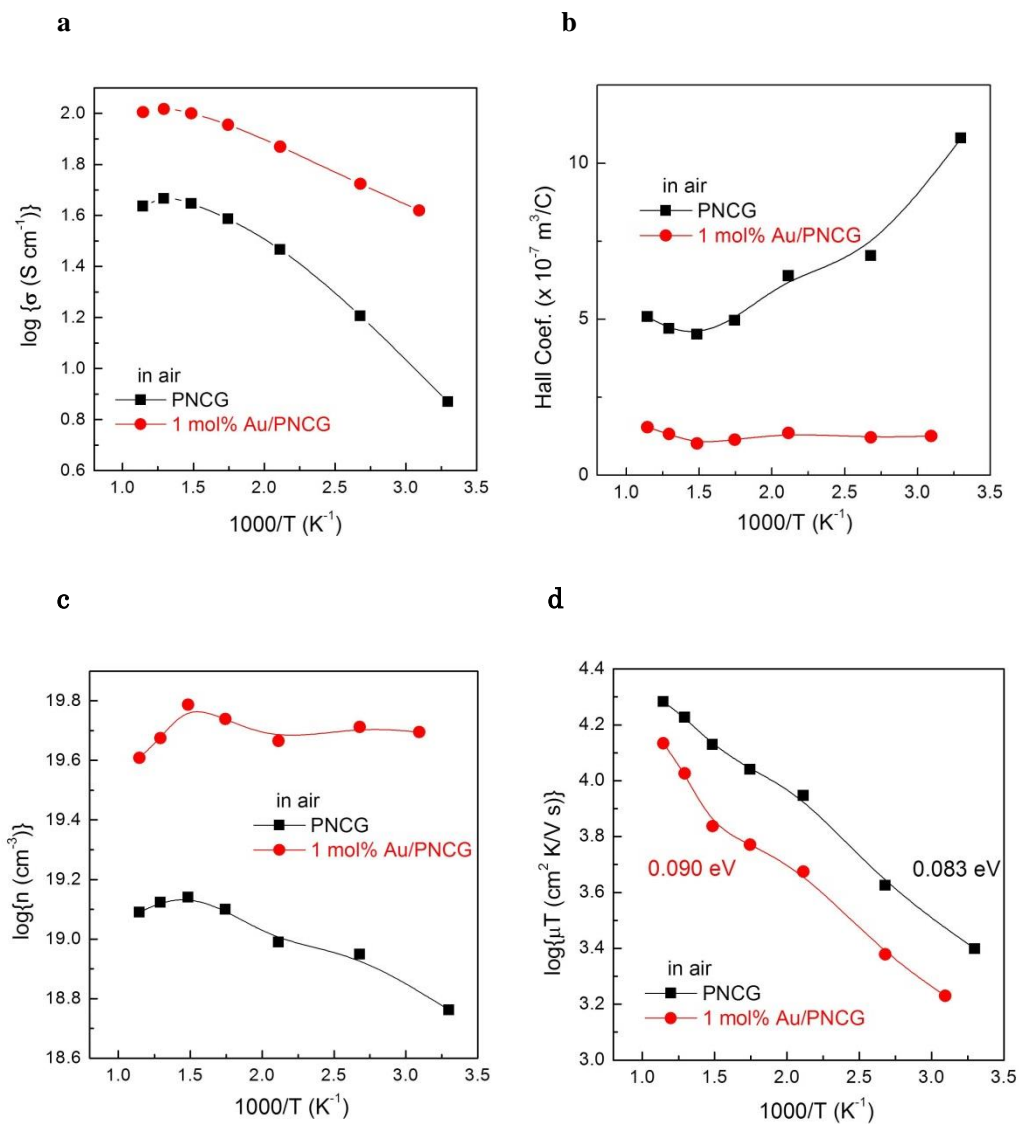
Figure S7 (corrected by density) Temperature dependence of Hall-effect measurement results for PNCG and 1 mol% Au/PNCG in air. (a) Electrical conductivity, (b) Hall coefficient, (c) electronic carrier concentration and (d) hole carrier mobility.

a

b

c

d
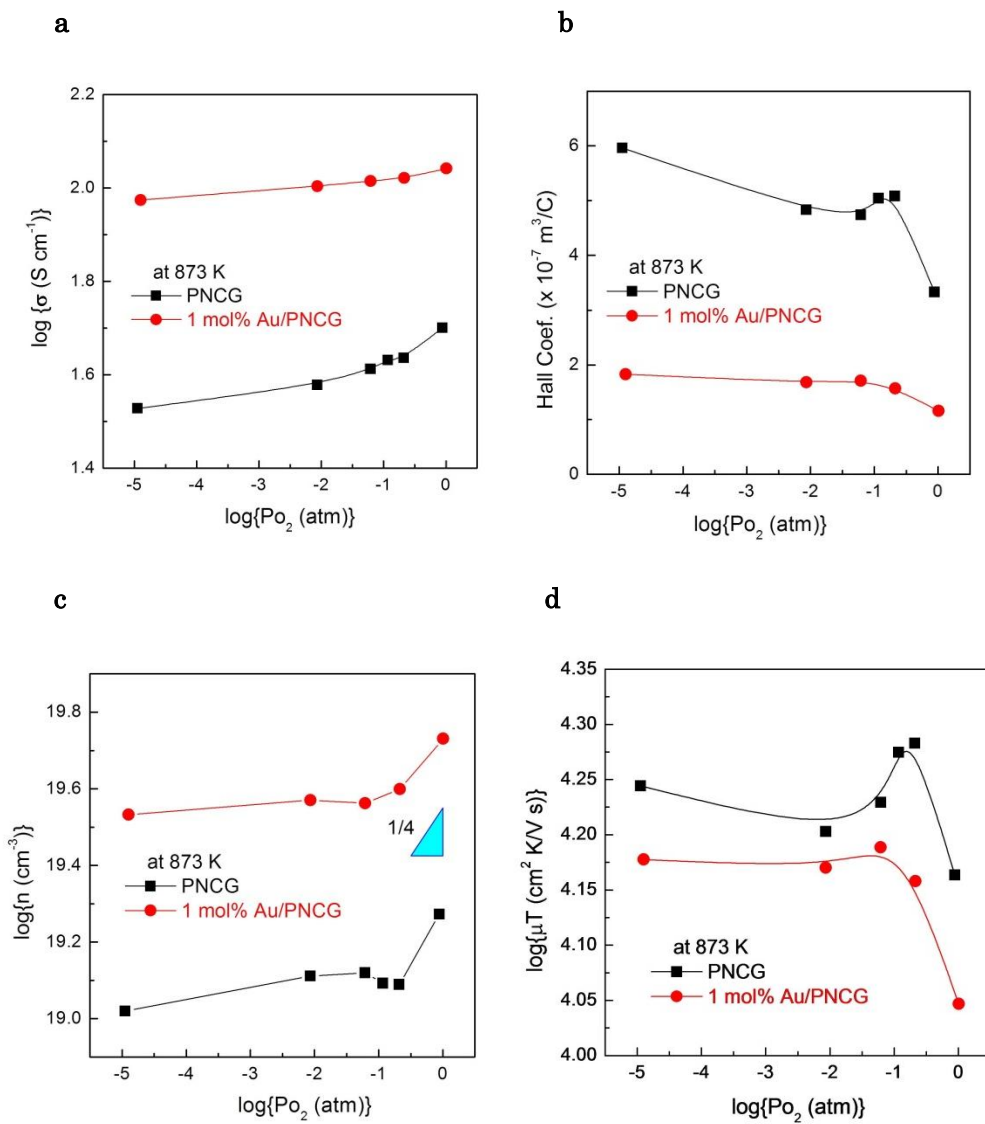
Figure S8 (corrected by density) Oxygen partial pressure dependence of the Hall-effect measurement results for PNCG and 1 mol% Au/PNCG at 873 K. (a) Electrical conductivity, (b) Hall coefficient, (c) electronic carrier concentration and (d) hole carrier mobility.

XPS measurements for Pr, Cu and O

For the Pr oxidation state, Pr-3d spectrum is normally used, and the BE positions of Pr-3d are 932 eV and 952 eV. However, the peak position of Cu-2p is exactly overlapped on this BE position, indicating the estimations of Pr and Cu valence number

are impossible to determine directly from the XPS spectrum for Pr-3d or Cu-2p. Therefore, we assume the Cu state is 2+, and estimate the valence number of Pr in the manuscript. Obtained values of Pr valence number in PNCG and 1 mol% Au/PNCG are exactly same as discussed in the manuscript. To prove this assumed valence number of Cu and estimated valence number of Pr, we compare the Pr-3d/Cu-2p spectra of PNCG and 1 mol% Au/PNCG. As shown in Figure S9, totally same spectra could be obtained, indicating that the state of Cu and Pr didn't change by three-dimensional strain. Therefore, this result supports that our assuming of Cu state and estimated Pr state in the manuscript are reasonable.
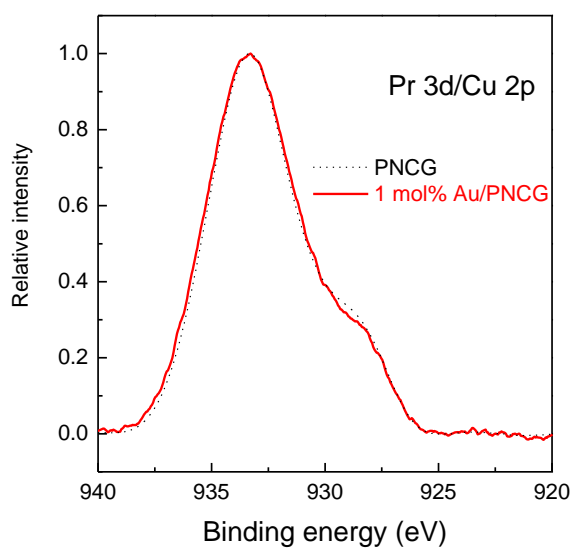
Figure S9. XPS spectra of overlapped Pr 3d/Cu 2p for PNCG and 1 mol% Au/PNCG.

The XPS spectra of O1s for PNCG and 1 mol% Au/PNCG were examined and are shown in Figure S10. The curve fitting results indicated the spectra are consisted with 3 peaks with the binding energy at 529.0 eV, 531.3 eV and 532.6 eV. By dispersing

the Au particles, the peak intensity at 529.0 eV and 532.6 eV increased, while the change of peak intensity at 531.3 eV was few. Considering the improved concentration of Ni^{3+} as described in the manuscript, the oxygen state with the Ni^{3+}-O bonding may be stronger since the coulomb interaction is larger than Ni^{2+}. This means binding energy for Ni^{3+}-O bonding is larger than that of Ni^{2+}-O. Therefore, increased intensity at the 532.6 eV could be assumed as the contribution of Ni^{3+}. Additionally, the low binding energy, which is at 529.0 eV, may be the contribution of interstitial oxide ions in PNCG. The K_2NiO_4 structure is well-known as the interstitial oxide ionic conductor at high temperature, indicating interstitial oxide ion easily mobile due to the weak bonding state compared with the other oxide ion sites. Although these discussions are hypothesis yet, the existence of both oxidized and reduced state of oxide ion seems to be a good agreement with the results in the manuscript. We will examine more details of bonding state of oxygen in the future.
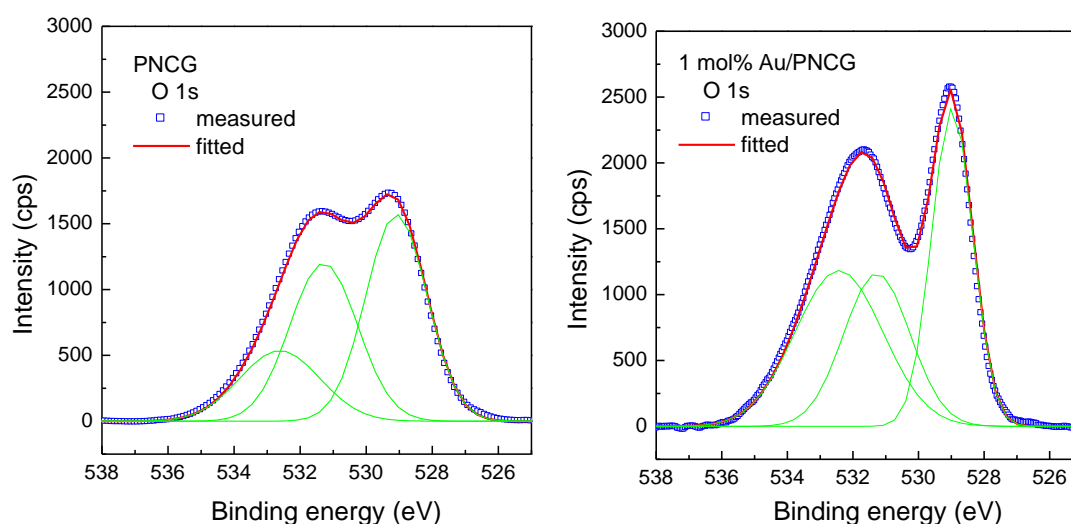
Figure S10 XPS spectra of O 1s for PNCG (left) and 1 mol% Au/PNCG (right).

References

(1) Allancon, C.; Gonthier-Vassal, A.; Bassat, J. M.; Loup, J. P.; Odier, P. Influence of oxygen on structural transitions in $Pr_2NiO_{4+\delta}$. *Solid State Ionics*, **1994**, *74*, 239‑248.

(2) Yashima, M.; Sirikanda, N.; Ishihara, T., Crystal Structure, Diffusion Path, and Oxygen Permeability of a Pr_2NiO_4-Based Mixed Conductor $(Pr_{0.9}La_{0.1})_2(Ni_{0.74}Cu_{0.21}Ga_{0.05})O_{4+\delta}$. *J. Am. Chem. Soc.* **2010**, *132*, 2385‑2392.

(3) Vashook, V. V.; Trofimenko, N. E.; Ulmann, H.; Makhnach, L. V. Oxygen nonstoichiometry and some transport properties of $LaSrNiO_{4-\delta}$ nickelate. Solid State Ionics, **2000**, *131*, 329‑336.

(4) Hücker, M.; Chung, K.; Chand, M.; Vogt, T.; Tranquada, J. M.; Buttrey, D. J. Oxygen and strontium codoping of La_2NiO_4: Room-temperature phase diagrams. Phys. Rev. B, **2004**, *70*, 064105.

(5) Williamson, G. K. & Hall, W. H. X-ray line broadening from field aluminium and wolfram. *Acta Metal* **1953**, *1*, 22-31.

(6) Nomura, K.; Takeuchi T.; Kamo, S.; Kageyama, H.; Miyazaki, Y. Proton Conduction in Doped $LaScO_3$ Perovskites. *Solid State Ionics* **2004**, *175* 553‑555.